Article

Modeling of Creep in Refractory Lining in Anode Baking Furnaces

Trond Brandvik [1,2,*], Louis Gosselin [3,4], Zhaohui Wang [5] and Tor Grande [2]

1   Hydro Aluminium AS, 3936 Porsgrunn, Norway
2   Department of Materials Science and Engineering, NTNU Norwegian University of Science and Technology, 7034 Trondheim, Norway; tor.grande@ntnu.no
3   Aluminum Research Centre REGAL, Quebec, QC G1V 0A6, Canada; louis.gosselin@gmc.ulaval.ca
4   Department of Mechanical Engineering, Université Laval, Quebec, QC G1V 0A6, Canada
5   SINTEF Industry, 7465 Trondheim, Norway; zhaohui.wang@sintef.no
*   Correspondence: trond.brandvik@hydro.com

Abstract: Refractory flue walls in anode baking furnaces are exposed to harsh conditions during operation, affecting the structural properties of the material. The flue walls in industrial furnaces degrade over time to the point where they no longer perform as intended and must be replaced. Earlier studies of spent refractory lining from anode baking furnaces have shown considerable densification of the flue wall bricks, where the densification varies significantly from the anode side to the flue side of the brick. The observed densification is proposed to be caused by high-temperature creep, and the aim of this work was to determine whether the uneven densification across the brick could be modeled using a finite element method (FEM) implementing high-temperature steady-state creep. Finite element modeling was used to model steady-state creep for a material similar to that used in the baking furnace. Thermal and physical parameters and boundary conditions were chosen to simulate the conditions in an anode baking furnace. Refractory samples of pristine and spent lining from the baking furnace were also analyzed with X-ray computed tomography (CT), with a reduction in the porosity confirming the densification during operation. The FEM modeling demonstrated that high-temperature creep could explain the observed densification in the spent flue walls. The present findings may be useful in relation to increasing the lifetime of industrial flue walls.

Keywords: anode baking furnace; refractory lining; FEM modeling; creep; densification

1. Introduction

The production of carbon anodes for aluminum electrolysis is an important part of the primary production of aluminum [1]. Petroleum coke, coal tar pitch, and recycled anode butts are mixed to form an anode paste, and compacted into the desired green anode shape, before being heat-treated in a baking furnace. In order to obtain anodes with the desired properties, a typical baking cycle lasts 14–17 days, during which the temperature varies between ambient and ~1250 °C. Refractory materials constitute the majority of the anode baking furnace, and the durability of the refractories, both structural and chemical, is crucial for the overall performance of the furnace. During baking, the temperature in the furnace is controlled by a flow of hot flue gas, continuously heated by the burning of hydrocarbons (liquified petroleum gas (LPG), natural gas (NG), etc.). The flue gas is separated from the anodes by hollow refractory walls. The cross section that separates the anode side from the flue side is the outer side of these flue walls. The width varies with the furnace technology (from 4 to 11 cm [2]), but its main function is similar. The finite element method (FEM) modeling reported in this study is focused on the simulation of the cross section of the flue wall. In addition to the structural requirements of the refractory lining, the ability to transport heat from the flue gas to the anodes is important. During years of operation, the flue walls are found to change, both microscopically and macroscopically [3–5]. The flue

walls bend, crack, and deform and the pits become narrower—at some point, even too narrow for the anodes to fit into the pits. This deformation of the walls leads to the ultimate need to replace flue walls, typically after 5–8 years, depending on the furnace design [3].

The main sources of the deformation, cracking, and corrosion of refractory materials are thermal stress, mechanical wear, and chemical corrosion [6]. Various investigations of spent lining from anode baking furnaces have been carried out in order to better understand the degradation of the refractory material [3,4,7–10]. Oumarou et al. measured the chemical composition, thermal properties, and density distribution across spent bricks [10]. They observed an increase in density at the anode side of the brick, and a reduction of density in the rest of the brick. No heat treatment of the samples prior to the investigation was performed, and it is inferred that open pores were filled with carbon deposition from the packing coke during operation of the furnace. Recent investigations of spent refractory lining have shown a significant variation in density and open porosity across the refractory wall, from the pit side towards the flue side [3]. The densification is also observed to be higher in the bottom part of the flue wall compared to the upper part of the wall. A reduction in density was observed after heat treatment of the spent lining in the laboratory, explained by the oxidation of the carbon previously deposited in the open porosity. A significantly higher density compared to the pristine material still remained after the heat treatment. No correlation between densification and increased sodium content in the flue wall was observed. Despite several attempts to explain the densification patterns observed in the refractory materials of anode baking furnaces, the densification mechanism remains to be determined.

The refractory wall is exposed to temperatures up to ~1250 °C during anode baking. The strong correlation of the densification and the vertical position in the wall points to the importance of gravimetric stress during baking induced by the weight of the wall itself. The refractoriness of the refractory materials is limited by high temperature creep, which results in structural deformation at elevated temperatures [11]. This suggests that plastic deformation by creep could be a potential mechanism explaining the reduction in porosity observed in the spent lining [11]. Creep is defined as a time-dependent permanent deformation of a solid material subjected to an elevated temperature at a stress level lower than the yield strength of the material [12]. Plastic deformation is normally taken into account as the temperature is approaching the material's softening point. At lower temperatures, as long as the material is not exposed to a load, significant deformation is not expected. Plastic deformation by creep becomes considerable when the material is exposed to a combination of elevated temperatures and an external load, especially over an extended period. Creep is usually divided into three stages, where the secondary creep stage describes the steady-state creep, the constant rate of deformation, often used when determining the lifetime of a material in a given application [13]. The primary and tertiary creep stages describe the deformation observed in the initial stage of the creep process and towards the time of failure, respectively. The steady-state creep rate can be found using the following expression:

$$\dot{\varepsilon} = A\sigma^n \exp\left(\frac{-Q}{RT}\right) \tag{1}$$

where $\dot{\varepsilon}$ is the creep rate or strain rate, σ is the stress level, T is the absolute temperature, R is the gas constant, and A, n, and Q are constants depending on the material. The stress exponent n is linked to the rate-controlling creep mechanism, where dislocation mechanisms ($1 \leq n \leq 4.5$), grain boundary sliding ($2 \leq n \leq 3$), and diffusion creep and vacancy flow ($n = 1$) are well-known mechanisms with the approximate range of stress exponent values indicated [14]. Creep data on similar refractory materials have been reported with stress exponent values ranging from 1.2 to 1.6 [15,16]. Mass transport by an amorphous intergranular phase is shown to have a stress exponent of 1.7, pointing to the plastic flow as the main mass transport mechanism [17]. The stress level in the wall is caused by the gravimetric forces from the wall itself. Q gives the thermal activation barrier and is therefore a particularly influential parameter for creep. The gradual increasing

gravimetrical force downwards in the furnace would induce an increasing creep rate downwards in the lining and, thus, a more pronounced densification. This correlates well with the autopsy findings in previous works [3].

The autopsy of spent linings also showed an uneven densification across the flue brick [3]. Close to the anode side, the densification was much more pronounced compared to the flue side, a behavior that was observed in the samples taken at three different heights. It was suggested that a gradient in the chemical potential of oxygen across the wall could possibly be related to this phenomenon. Investigations of coal ash slags show a reduction in viscosity when exposed to low partial pressures of oxygen [18,19]. Measurements of the pit gas atmosphere have demonstrated the reducing nature of the pit atmosphere compared to the oxidizing flue gas [20]. Moreover, the stability of perovskite oxides in reducing atmosphere has been investigated, showing that oxygen deficiency and, finally, decomposition take place at sufficiently low oxygen partial pressures [21,22]. Creep in yttria-doped ceria is also known to increase with decreasing oxygen partial pressure [23]. The significant gradient in oxygen activity could, thus, have an important influence on the creep rate across the bricks.

The aim of this work was to investigate whether the observed deformation of refractory lining could be described by the creep mechanism at elevated temperatures using an FEM model. The creep mechanism for the observed densification was inferred in previous studies, and the aim was to investigate whether deformation of the flue wall could be described by a creep mechanism. Potential measures to avoid the densification can be taken knowing the material's deformation mechanism. Steady-state creep data for relevant materials have been reported, forming the basis for the present modeling. Finite element method (FEM) modeling was used to simulate strain in the refractory lining, and the results are discussed in relation to the densification of the wall reported in previous work [3]. To confirm the reduction in porosity, X-ray tomography was applied to the samples investigated in the previous study [3].

2. Materials and Methods

2.1. X-Ray Computed Tomography (CT)

Samples of refractory lining from the bottom of the pit in an open-top baking furnace were characterized by X-ray computed tomography (CT). Core samples 20 mm in diameter were taken from each side of the refractory cross section separating the anode side from the flue side. The CT analysis was carried out with a Nikon XT H225 ST instrument using a molybdenum X-ray source (Nikon Corporation, Tokyo, Japan). Imaging was performed at 185 kV and 60 μA, resulting in 3141 recorded projections per revolution with a speed of 0.707 projections per second. The resolution of the analysis, i.e., the voxel size (combination of "volume" and "pixel") in each dimension, was 11.2 μm. Post processing of images was carried out in ImageJ (version 1.51).

### 2.2. Finite Element Method (FEM) Modeling

The creep model developed with finite element software is described below. The domain consisted of a 2D slice of a brick subjected to different load conditions depending on its position in the furnace wall. Creep is a phenomenon occurring only at elevated temperatures, and to simulate creep during anode baking, only the time above a certain temperature threshold is considered. To reduce the computational time, the temperature was fixed at 1100 °C during the simulations. This is a simplification of the actual temperature regime in the baking furnace, which varies with time and can reach 1150 °C to 1200 °C for shorter periods during baking. For each baking cycle, the temperature is above 1100 °C for approximately 30 h [20]. The creep rate is thermally activated and fixing the temperature to 1100 °C is therefore a simplification of the actual creep rate during operation. This is discussed in relation to the other parameters later. The wall investigated in this paper had experienced 160 cycles [3], resulting in approximately 4800 h at temperatures above the set threshold. This gives an indication of the necessary time length of the simulation.

2.2.1. Description of the Model

In the FEM model, porosity is introduced as cavities in a homogeneous material. The cavities are randomly distributed, adding up to a total porosity corresponding to the observed open porosity of the pristine refractory material (i.e., 17%). The apparent density of the model includes the internal porosity, and a reduction in porosity leads to an increase in the apparent density. The removal of porosity is based on the secondary creep mechanism, described by Equation (1).

The model was implemented with the software COMSOL 5.4, using the module for Structural Mechanics, including the module for Non-linear Structural Materials. The mesh sequence type was set to Physics-controlled mesh, and the mesh size was set to Normal.

A 2D geometry was chosen and is summarized in Figure 1. Here, the cross section of the refractory brick (12 cm × 7.5 cm), from the anode side (left) to the flue side (right), is illustrated with its porosity for all sections. The porosity was introduced as circles with constant radius in the model, randomly distributed across the geometry. To investigate the effect of pore size, three values of the pore radius were studied: 0.5 mm, 1 mm, and 2 mm. For all cases, the initial total porosity was kept equal to the pristine open porosity. The geometry was divided into three regions (Regions 1, 2, and 3), as shown in Figure 1, allowing different creep parameters in each region of the domain. Each region can be assigned a different value for the pre-exponential factor, *A*, to represent different oxygen activity across the refractory. The model can be used to simulate different vertical positions in the wall (i.e., top, middle, and bottom sections) by adjusting the value of the gravimetric stress applied as a boundary condition. The applied stress is calculated from the weight of the bricks above the position considered.
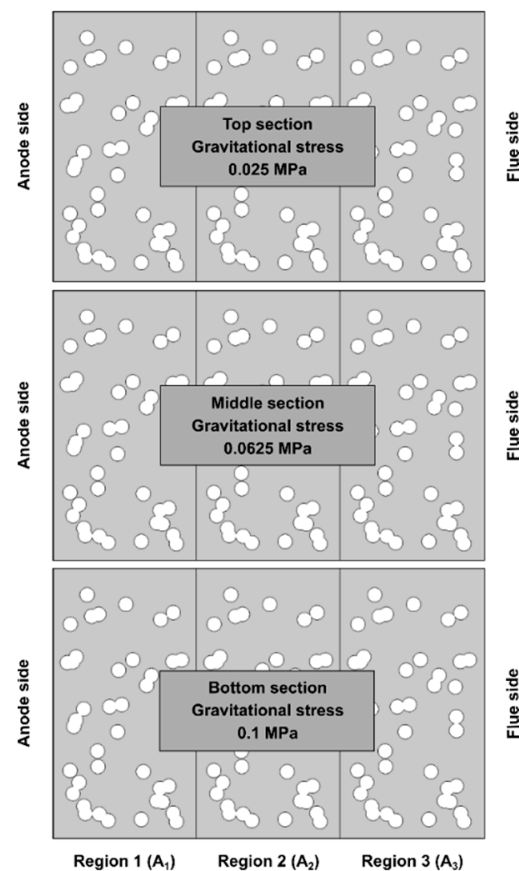
Figure 1. Illustration of the geometry used in the modeling, with pore size of 2 mm. The geometry is divided into three regions with different values of the pre-exponential factor in Equation (1). The gravimetric stress for each section is given. Reprinted with permission from [2], Brandvik, 2019.

Two cases were investigated using the model, with variations in the boundary conditions. In Case 1, all vertical boundaries were allowed vertical displacement, but not horizontal displacement (prescribed displacement: $u_x = 0$). In Case 2, the two outermost vertical boundaries were allowed vertical displacement, but not horizontal displacement. The two internal vertical boundaries were free to move in both directions. The bottom boundary was kept fixed for both cases, while the top boundary was exposed to a boundary force simulating the pressure from the bricks above in the wall. Densification in the refractory wall has been reported [2], where the bottom samples were collected 1 m above the pit floor, the top samples 1 m below the packing coke, and the middle samples at the midway between the two others. With a total height of 5 m and a density of 2.4 g/cm^3, the pressure from the wall at these sampling positions were calculated. The top, middle, and bottom sections were exposed to an approximate pressure of 0.025 MPa, 0.0625 MPa and 0.1 MPa, respectively.

The material properties used in the finite element modeling are presented in Table 1. The values are based on literature data from similar materials.

Table 1. Data used in the FE modeling. Literature data for comparison.

| Property	Literature Value	Values Used in Simulations	Unit	References
E	2–15	10	GPa	[24–27]
Q	450–500	485	kJ mol^{-1}	[15,28]
n	1.2–1.6	1.2	[-]	[15]
A (Region 1)	10^{11}–10^{12}	3×10^{11}	[-]	[15]
A (Region 2)	10^{11}–10^{12}	8×10^{10}	[-]	[15]
A (Region 3)	10^{11}–10^{12}	3×10^{10}	[-]	[15]

2.2.2. Material Properties Used in the Model

Young's modulus (E), thermal activation barrier for creep (Q), pre-exponential factor (A), density (r), and stress exponent (n) are important input parameters in the modeling of the behavior of the refractory material in the model. The density of the refractory material has been reported in earlier work [3]. Young's modulus values in the range of 2 GPa to 15 GPa [24–27] (testing temperature varying from room temperature to 1200 °C) have been reported for similar materials. Creep data for similar materials have been reported as 330–500 kJ/mol for the thermal activation barrier [15,28], 1.2 to 1.6 for the stress exponent [15,16], and 10^{11} to 10^{12} for the pre-exponential factor [15].

Based on the properties of coal ash slags, and the changing stability of certain perovskites and yttria-doped ceria at varying partial pressures of oxygen [18,19,21–23], it is suggested that the reducing atmosphere has a destabilizing effect on the refractory lining, causing an increased creep rate at reducing conditions. This is implemented in the model by separating the geometry into three regions (Figure 1), each assigned with a different creep behavior. The pre-exponential factor is set to a larger value on the anode side to yield a higher creep rate (Region 1), and close to the flue side, a smaller pre-exponential factor is imposed, leading to a lower creep rate (Region 3). Both values were tuned to obtain a good correlation with one of the data sets in the experimental data, as described in Appendix A.

2.2.3. Determination of the Change in Porosity for the Model

The change in the porosity in the model was calculated by the displacement of the boundaries surrounding the given region of the geometry. The area of the model elements itself does not change during the simulations, and the constitutive law used does not directly account for changes in density. The deformation occurring during the simulations causes the area representing the internal porosity to be reduced. Since the geometry deforms in a downward manner due to creep, the increase in the area on top of the geometry is equal to the reduction in internal pore area, as illustrated in Figure 2. By measuring the average displacement of the top boundary multiplied by the width of the geometry, the change

in the pore area is determined and, hence, the change in relative porosity, as presented in Figure 2.
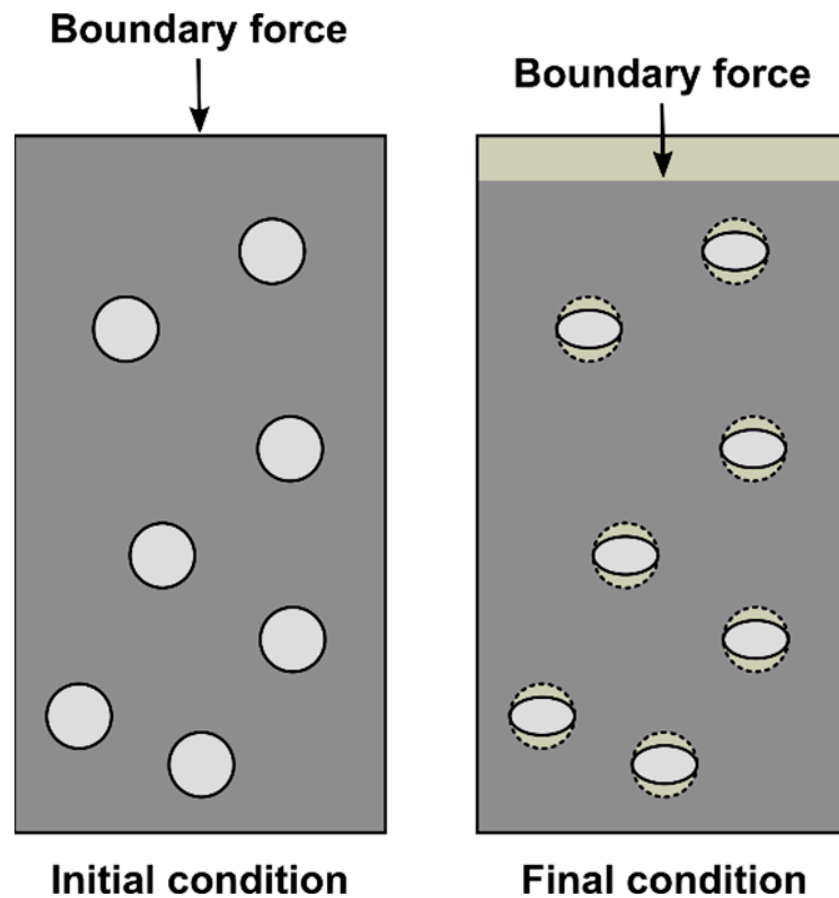
Figure 2. Illustration of the redistribution of porosity occurring during the simulation. The geometry deforms in a downward manner, and the reduction in the internal pore area corresponds to the area above the geometry after modeling. Reprinted with permission from [2], Brandvik, 2019.

3. Results

3.1. Porosity and Distribution of Pores in Spent Refractory Lining

Lining from the bottom section of the open-top baking furnace was investigated by X-ray computed tomography (CT). Samples were taken from the furnace during the replacement of the flue walls. The CT images of the material at the anode and flue side are presented in Figures 3 and 4. The level of porosity is clearly lower at the anode side (a) relative to the flue side (b). Most of the reduction in porosity is found in the binder phase, where the pores are small. This is also expected, since the plastic deformation and sintering are most likely to take place in the region with small grains and higher content of amorphous phase.

3.2. Modeling

Simulations for geometries with a pore radius of 0.5 mm, 1 mm, and 2 mm were carried out for Case 1 and Case 2. For each case, three gravimetrical stress levels were applied to the top boundary to simulate the external pressure working on the bricks in the top, middle, and bottom section of the wall. As the top boundary force increases, the degree of deformation increases correspondingly. In Figure 5, the deformed geometry after simulation (5000 h at 1100 °C) together with the corresponding stress distribution is shown for the geometry with a 2 mm pore size. The scale bar ranges from zero to 0.2 MPa for all three geometries. The buildup of stress is in general low but increases as the

gravimetric stress increases. The top section with 0.025 MPa applied to the top boundary shows no significant stress buildup. For the middle section, with 0.0625 MPa applied to the top boundary, the stress becomes significant. The buildup is, however, larger in Region 3 compared to Region 1, due to the lower creep rate in Region 3. In Region 1, the creep allows the material to relax under the top boundary stress, causing a reduction in stress buildup. In the bottom section, for a top boundary stress of 0.1 MPa, the difference between Region 1 and Region 3 becomes even more distinct. There is also a significant concentration of stress at the pore surfaces.
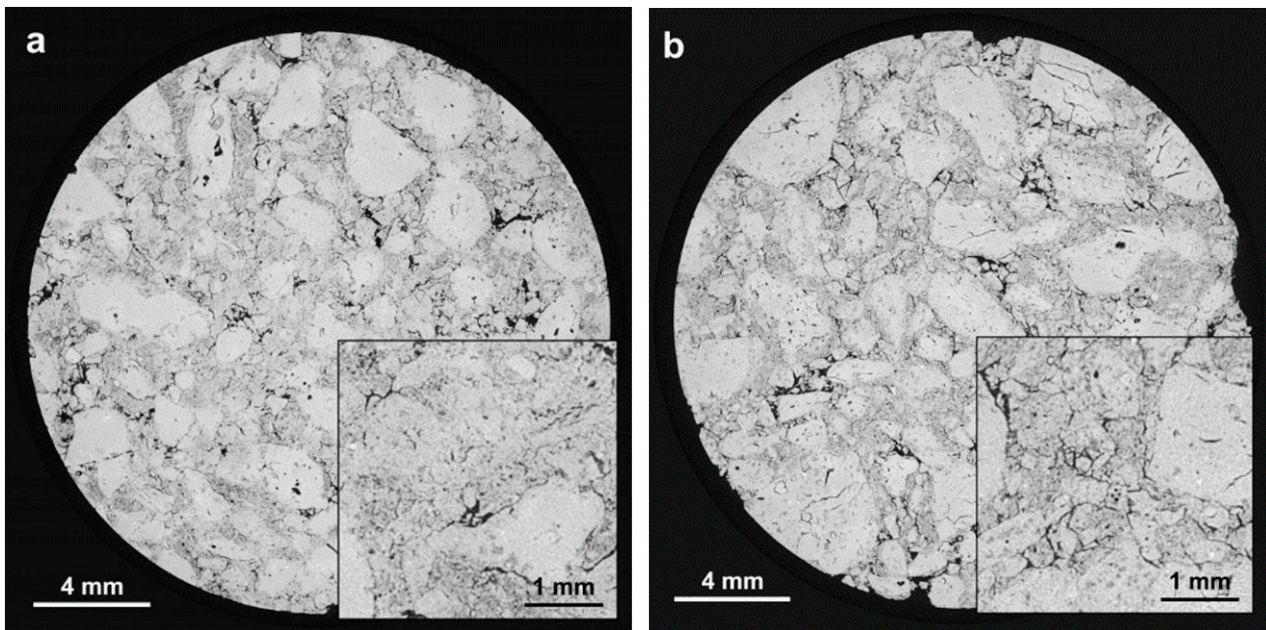
Figure 3. X-ray tomography of refractory lining at the (**a**) anode side and (**b**) flue side. The refractory material is shown in gray and the pores shown in black. Reprinted with permission from [2], Brandvik, 2019.
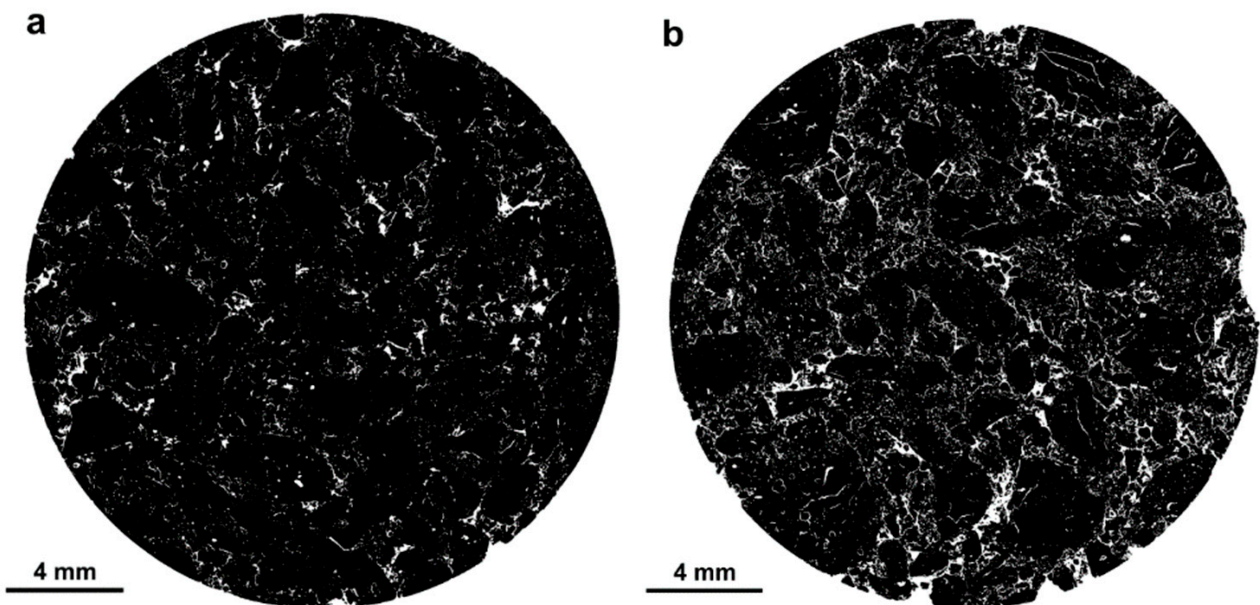

Figure 4. X-ray tomography of refractory lining at the (**a**) anode side and (**b**) flue side. The refractory material is shown in black, and the pores shown in white. The reduction in porosity in the bonding phase between the large grains is clearly visible. Reprinted with permission from [2], Brandvik, 2019.

    The variation in the porosity for all simulations of both cases is presented in Figure 6. The simulations are plotted together with the experimental data from the autopsy work [3]. The variation in the porosity obtained by the FEM modeling is in good agreement with the experimental data. The variation in densification as a function of pore size is, however, not significant, and the creep behavior does not seem to be largely affected by the change in pore size. The small variations observed between the three pore sizes for each case could be related to the randomized distribution of pores, as the locations of the pores in the material could affect the creep rate to some degree. Here, it is important to note that the material is considered homogeneous without any effect of the grain size, particularly the coarse grains in the refractory material. The actual refractory material used in the industry has a wide particle size distribution, which is a crucial part of the material design. The pore size distribution, on the other hand, does not affect the high-temperature properties of the material to any significant degree. This corresponds with the results from the current results.
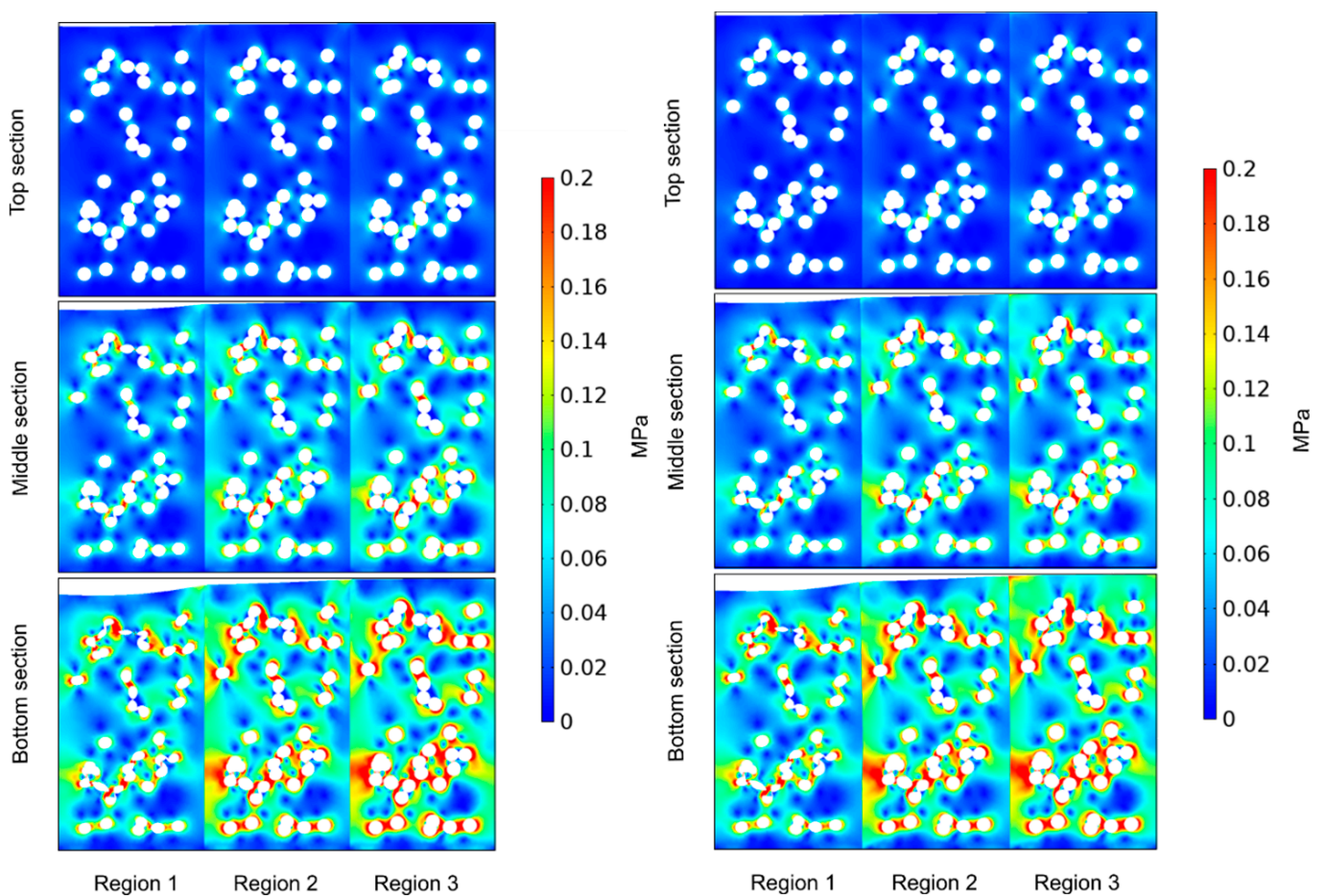
Figure 5. Deformed geometries with their corresponding stress distribution after 5000 h at 1100 °C for 2 mm pore size. Case 1 (**left**) and Case 2 (**right**). The three sections (top, middle, and bottom) have an increasing degree of pressure on the top boundary (0.025 MPa, 0.0625 MPa, and 0.1 MPa, respectively). The stress concentration is highest in the bottom section where the pressure is the largest. Region 1 is observed to deform to a larger degree compared to Region 2 and 3, resulting in some relaxation in the material and, therefore, a reduction in the stress concentration. Reprinted with permission from [2], Brandvik, 2019.
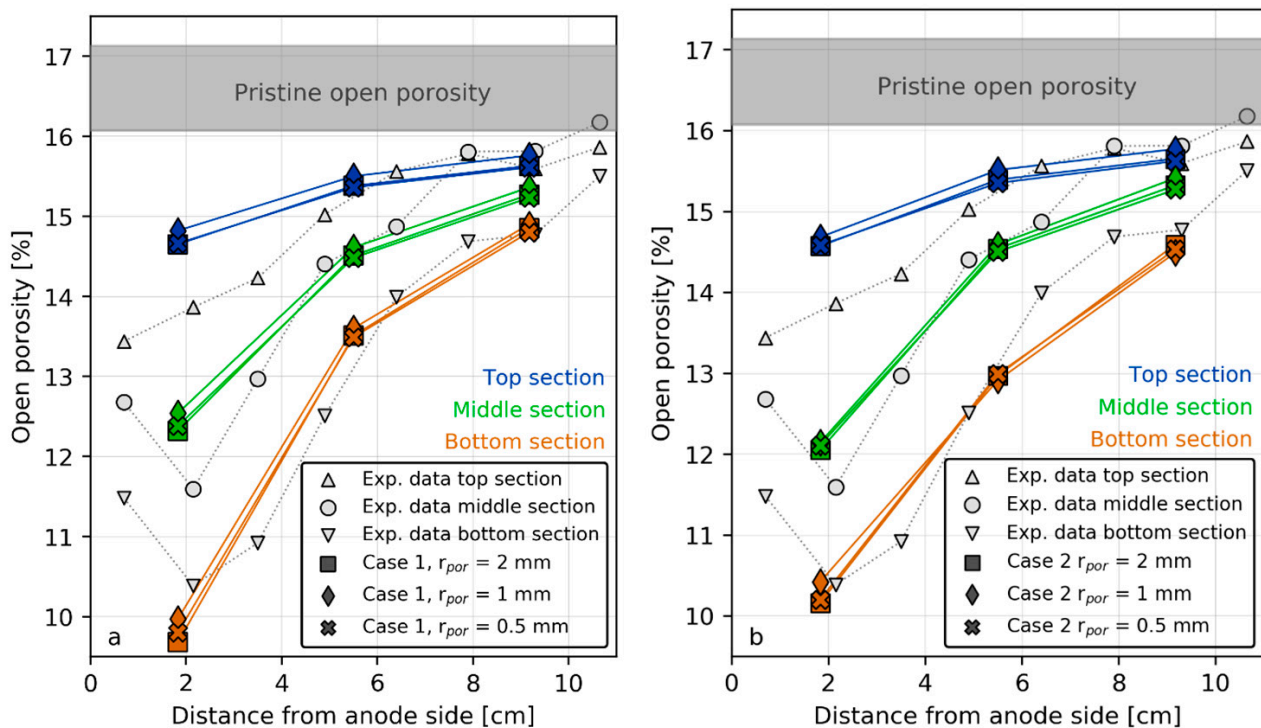
Figure 6. Porosity for all simulations of Case 1 (**a**) and Case 2 (**b**). The results from the modeling is compared to the experimental data from Brandvik et al. [2]. The chemical composition of the samples from the experimental work is Al_2O_3 (49.5 wt%), SiO_2 (44.5 wt%), Fe_2O_3 (0.9 wt%), TiO_2 (≤ 1.4 wt%), and $Na_2O + K_2O$ (0.4 wt%). Reprinted with permission from [2], Brandvik, 2019.

4. Discussion: Creep as a Densification Mechanism

Two important observations can be made from the FEM simulations. First, the gravimetric stress is generally large enough to result in a considerable reduction in the open porosity at a reasonable temperature and duration. The temperature used in the simulations is moderate compared to the maximum temperature measured during operation in the industry, taking the high activation energy and thermal activation of creep into account. The lining is, thus, exposed to a stress level during anode baking that is sufficient to cause significant creep in the refractory wall. Second, the variation in the creep as a function of increasing gravimetric stress correlates well with the experimental data, demonstrating a reduction in the open porosity. This is also clearly evident from X-ray tomography (Figures 3 and 4). By focusing on one region corresponding to a fixed pre-exponential parameter, a gradient in the porosity is induced by the gradual increase in gravimetric stress. The finite element method simulations therefore support creep as the dominating mechanism for the observed reduction in the open porosity.

The pre-exponential factor used in the modeling varies from 3×10^{10} to 3×10^{11} from the flue side to the anode side. This change in the creep rate corresponds to a reduction in the thermal activation barrier (Q) from 485 kJ/mol to 459 kJ/mol. This is a significant reduction in the Q parameter, showing that there is potentially a considerable difference in thermomechanical performance of the refractory lining at the anode side compared to the flue side. The product between the pre-exponential factor and the exponential expression in the creep equation, $A \cdot \exp\left(\frac{-Q}{RT}\right)$, will always be constant at isothermal conditions. Choosing Q as the tunable parameter over A would therefore have yielded the same result. Fixing the temperature at 1100 °C was a simplification of the actual temperature regime in the furnace. The creep rate is given by the product of factors in the creep equation $\left(A \cdot \exp\left(\frac{-Q}{RT}\right)\right)$, and choosing higher temperature would have been compensated for by reducing the pre-exponential factor, A, or increasing the thermal activation barrier, Q.

The findings from the modeling show that the density generally increases with increasing gravimetric stress, and this corresponds well with the experimental data reported from the autopsies [2]. The results from the modeling supports the idea that creep is the dominating densification mechanism in the refractory materials in anode baking furnaces.

A reducing atmosphere is proposed to have a destabilizing effect on the refractory lining, leading to low partial pressure of oxygen affecting the refractoriness of the material to a considerable degree. In traditional refractories, a broad grain size distribution is crucial for high refractory performance, where the large grains, usually several millimeters in size, give structural stability to the material, while the smaller grains fill the voids and bind the material together. The CT images in Figures 3 and 4 show that most of the reduction in open porosity is observed in the bonding phase where the pores and grains are small. The large grains are not significantly affected by the creep process, but the smaller grains and pores in the binder phase are redistributed and compacted during creep. The effect of reducing atmosphere on creep rate in refractory materials should be investigated more thoroughly, with the partial pressure of Oxygen (pO_2) and grain size distribution as varying parameters. By obtaining more knowledge on these relations, it may be possible to tailor the microstructure of the materials in the lower part of the flue wall to mitigate creep in this area of the lining.

5. Conclusions

The densification observed in industrial anode baking flue walls has previously not been described using an FEM simulation. A finite element model of refractory material was developed and used to demonstrate that high-temperature creep can indeed explain the densification observed in the lining in anode baking furnaces. The modeling was carried out with parameters representing the thermal history of the samples collected in autopsies of industrial furnaces. The study demonstrated that secondary (steady-state) creep could be used to model the densification observed in samples from industrial anode baking furnaces. Samples of both pristine and spent refractory lining were analyzed using X-ray computed tomography (CT), showing a significant difference in porosity between the anode side and the flue side. The results from the CT analysis support the modeling, demonstrating that high-temperature creep could account for the observed densification of refractory lining in anode baking furnaces.

Appendix A. Determination of Reduction in Porosity

Once the temperature, duration of the simulation, stress exponent (*n*), and creep activation barrier (*Q*) were fixed, the only parameter left was the pre-exponential factor (*A*). The pre-exponential parameter in the creep equation (Equation (1)) was tuned to correlate with the experimental data of measured open porosity in spent refractory lining. Open porosity from Region 1 (stress level of 0.1 MPa) was used to find a corresponding pre-

exponential factor. The same procedure was carried out for Region 3, with experimental data from the flue side. The difference in the chemical environment at the anode side and the flue side is proposed to have an impact on the creep rate. The pre-exponential factor for Region 2 was therefore chosen as the value midway between the pre-exponential factor determined for Region 1 and Region 3. Then, the modeling was repeated for stress levels of 0.025 MPa and 0.0625 MPa, with the remaining parameters kept constant.

References

1. Prigent, P.; Bouchetou, M.L.; Poirier, J.; Hubert, P. The effect of the addition of fine andalusite particles in refractory bricks on gaseous corrosion. *JOM* **2008**, *60*, 58–63. [CrossRef]
2. Brandvik, T. Degradation of Refractory Lining in Carbon Anode Baking Furnaces. Ph.D. Thesis, NTNU Norwegian University of Science and Technology, Trondheim, Norway, 2019.
3. Brandvik, T.; Wang, Z.; Ratvik, A.P.; Grande, T. Autopsy of refractory lining in anode kilns with open and closed design. *Int. J. Appl. Ceram. Technol.* **2019**, *16*, 602–613. [CrossRef]
4. Brunk, F. Corrosion and behaviour of fireclay bricks varying chemical composition used in bottom lining of reduction cells. In Light. Metals; TMS, San Fransisco, USA, 1994; pp. 477–482.
5. Prigent, P.; Bouchetou, M.L. Gaseous corrosion of aluminosilicate refractories in anode baking furnaces used for aluminium production part 1. *Interceram* **2009**, *58*, 121–126.
6. Cui, K.; Mao, H.; Zhang, Y.; Wang, J.; Shen, F. Microstructure and corrosion behavior of Al_2O_3-Cr_2O_3 composites with various Cr_2O_3 content in Al_2O_3-SiO_2-CaO-FeO slag. *Ceram. Int.* **2022**, *48*, 35555–35567. [CrossRef]
7. Butter, J.; Bongers, A. Alterations of anode baking furnace bricks during operation. In *Light Metals*; TMS: Las Vegas, NV, USA, 1995; pp. 633–639.
8. Brandvik, T.; Ratvik, A.P.; Wang, W.; Grande, T. Investigations of spent refractory lining in an anode baking furnace. In *Light. Metals*; Springer International Publishing: Cham, Switzerland, 2017; pp. 1281–1288.
9. Brandvik, T.; Ratvik, A.P.; Grande, T. Thermodynamic assessment of the chemical durability of refractory lining in anode baking furnaces. In Proceedings of the 34th Conference and Exhibition ICSOBA, Quebec City, QC, Canada, 3–6 October 2016.
10. Oumarou, N.; Kocaefe, D.; Kocaefe, Y. Investigation of the refractory bricks used for the flue wall of the horizontal anode baking ring furnace. *Ceram. Int.* **2016**, *42*, 18436–18442. [CrossRef]
11. Luz, A.P.; Lopez, S.J.S.; Gomes, D.T.; Pandolfelli, V.C. High-alumina refractory castables bonded with novel alumina-silica-based powdered binders. *Ceram. Int.* **2018**, *44*, 9159–9167. [CrossRef]
12. Li, J.; Mattila, T.; Vuorinen, V. MEMS Reliability. In *Handbook of Silicon Based MEMS Materials and Technologies*, 2nd ed.; Elsevier Inc.: Amsterdam, The Netherlands, 2015; pp. 744–763.
13. Richerson, D.W. Time, temperature and environmental effects on properties. In *Modern Ceramic Engineering*, 3rd ed.; Taylor & Francis Group CRC Press: Boca Raton, FL, USA, 2006; pp. 243–283.
14. Langdon, T.G. Identifying creep mechanisms in plastic flow. *Int. J. Mater. Res.* **2005**, *96*, 522–531. [CrossRef]
15. Borovkova, L.B.; Lukin, E.S.; Poluboyarinov, D.N. Creep of aluminosilicate refractories. *Ogneupory* **1969**, *7*, 39–43. [CrossRef]
16. Torrecillas, R.; Calderon, J.M.; Moya, J.S.; Reece, M.J.; Davies, C.K.L.; Olagnon, C.; Fantozzi, G. Suitability of mullite for high temperature applications. *J. Eur. Ceram. Soc.* **1999**, *19*, 2519–2527. [CrossRef]
17. Jin, Q.; Wilkinson, D.S.; Weatherly, G.C. High-resolution electron microscopy investigations of viscous flow creep in high-purity silicon nitride. *J. Am. Ceram. Soc.* **1999**, *82*, 1492–1496. [CrossRef]
18. Cao, X.; Kong, L.; Bai, J.; Ge, Z.; He, C.; Li, H. Effect of water vapor on coal ash slag viscosity under gasification conditions. *Fuel* **2019**, *237*, 18–27. [CrossRef]
19. Wu, X.; Zhang, Z.; Piao, G.; He, X.; Chen, Y.; Kobayashi, N. Chinese coal ash melting during char-CO_2/H_2O gasification reaction. *Energy Fuels* **2009**, *23*, 2420–2428. [CrossRef]
20. Brandvik, T.; Gaertner, H.; Ratvik, A.P.; Grande, T.; AArhaug, T.A. In situ monitoring of pit gas composition during baking of anodes for aluminium electrolysis. *Met. Mater. Trans. B* **2019**, *50B*, 950–957. [CrossRef]
21. Nakamura, T.; Petzov, G.; Gauckler, L.J. Stability of the perovskite phase LaBO3 (B = V, Cr, Mn, Fe, Co, Ni) in the reducing atmosphere. *Mater. Res. Bull.* **1979**, *14*, 649–659. [CrossRef]
22. Pecchi, G.; Campos, C.; Peña, O. Thermal stability against reduction of LaMn(1-y)$Co_y$$O_3$ perovskites. *Mater. Res. Bull.* **2009**, *44*, 846–853. [CrossRef]
23. Iguchi, F.; Endo, Y.; Ishida, T.; Ykobori, T.; Yugami, H.; Otake, T. Oxygen partial pressure dependence of creep on yttria-doped ceria ceramics. *Solid. State Ion.* **2005**, *176*, 641–644. [CrossRef]
24. Amrane, B.; Ouedraogo, E.; Mamen, B.; Djaknoun, S.; Mesrati, N. Experimental study of the thermo-mechanical behaviour of alumina-silicate refractory materials based on a mixture of algerian kaolinitic clays. *Ceram. Int.* **2011**, *37*, 3217–3227. [CrossRef]
25. Osendi, M.I.; Baudin, C. Mechanical properties of mullite materials. *J. Eur. Ceram. Soc.* **1996**, *16*, 217–224. [CrossRef]
26. Mong, L.E. Elastic behavior and creep of refractory bricks under tensile and compressive loads. *J. Res. Nat. Bur. Stand.* **1949**, *38*, 229. [CrossRef]

27. Panferov, V.M.; Korol, E.Z.; Pitak, N.V.; Turchinova, L.N.; Ansimova, T.A. Thermomechanical properties of mullite-corrundum refractories. *Ogneupory* **1983**, *7*, 20–24.
28. Sokolova, L.V.; Bakunov, V.S. Creep in aluminosilicate materials. *Keramika* **1983**, *5*, 18–20. [CrossRef]